# Aldosterone controls primary cilium length and cell size in renal collecting duct principal cells

Komarynets, Olga; Chassot, Alexandra; Bernabeu Dizin, Eva; Czogalla, Jan; Monnay, Isabelle; Liaudet, Nicolas; Prodon, François; Loffing, Johannes; Feraille, Eric

**How to cite**

KOMARYNETS, Olga et al. Aldosterone controls primary cilium length and cell size in renal collecting duct principal cells. In: FASEB Journal, 2020, vol. 34, n° 2, p. 2625–2640. doi: 10.1096/fj.201901947R

This publication URL: https://archive-ouverte.unige.ch/unige:140143
Publication DOI: 10.1096/fj.201901947R

Received: 3 August 2019 | Revised: 20 November 2019 | Accepted: 5 December 2019

DOI: 10.1096/fj.201901947R

RESEARCH ARTICLE

THE FASEB JOURNAL

# Aldosterone controls primary cilium length and cell size in renal collecting duct principal cells

**Olga Komarynets[1] | Alexandra Chassot[1] | Eva Bernabeu[1] | Jan Czogalla[2] | Isabelle Roth[1] | Nicolas Liaudet[3] | François Prodon[3] | Johannes Loffing[2] | Eric Feraille[1]**

[1]Department of Cell Physiology and Metabolism, Faculty of Medicine of Geneva, University Medical Center, University of Geneva, Geneva, Switzerland

[2]Institute of Anatomy, University of Zürich, Zürich, Switzerland

[3]Service of Bioimaging, University of Geneva, Geneva, Switzerland

**Correspondence**
Eric Feraille, Department of Cell Physiology and Metabolism, Faculty of Medicine of Geneva, University Medical Center, 1 rue Michel Servet, CH-1211 Geneva 4, Switzerland.
Email: Eric.Feraille@unige.ch

**Funding information**
National Center of Competence in Research Kidney Control of Homeostasis and Swiss National Science Foundation, Grant/Award Number: 31003A_156736/1 and 31003A_175471/1; Fondation Ernst et Lucie Schmidheiny

## Abstract

Primary cilia are nonmotile sensory organelles found on the surface of almost all kidney tubule epithelial cells. Being exposed to the tubular lumen, primary cilia are thought to be chemo- and mechanosensors of luminal composition and flux, respectively. We hypothesized that, $Na^+$ transport and primary cilia exist in a sensory functional connection in mature renal tubule epithelial cells. Our results demonstrate that primary cilium length is reduced in mineralocorticoid receptor (MR) knockout (KO) mice in a cell autonomous manner along the aldosterone-sensitive distal nephron (ADSN) compared with wild type (as μm ± SEM; 3.1 ± 0.2 vs 4.0 ± 0.1). In mouse cortical collecting duct $(mCCD)_{cl1}$ cells, which are a model of collecting duct (CD) principal cells, changes in $Na^+$ transport intensity were found to mediate primary cilium length in response to aldosterone (as μm ± SEM: control: 2.7 ± 0.9 vs aldosterone treated: 3.8 ± 0.8). Cilium length was positively correlated with the availability of IFT88, a major intraflagellar anterograde transport complex B component, which is stabilized in response to exposure to aldosterone treatment. This suggests that the abundance of IFT88 is a regulated, rate limiting factor in the elongation of primary cilia. As previously observed in vivo, aldosterone treatment increased cell volume of cultured CD principal cells. Knockdown of IFT88 prevents ciliogenesis and inhibits the adaptive increase in cell size that was observed in response to aldosterone treatment. In conclusion, our results reveal a functional connection between $Na^+$ transport, primary cilia, and cell size, which may play a key role in the morphological and functional adaptation of the CD to sustained changes in active $Na^+$ reabsorption due to variations in aldosterone secretion.

**KEYWORDS**

aldosterone, cell volume, collecting duct, primary cilium, sodium

**Abbreviations:** 17-OHP, 17-hydroxyprogesterone; ADPKD, autosomal dominant polycystic kidney disease; AQP2, aquaporin-2; ARPKD, autosomal recessive polycystic kidney disease; ASDN, aldosterone-sensitive distal nephron; CD, collecting duct; CHX, cycloheximide; CNT, connecting tubule; DCT, distal convoluted tubule; ENaC, epithelial $Na^+$ channels; GFR, glomerular filtration rate; IFT, intraflagellar transport; mCCD, mouse cortical collecting duct; MDCK, Madin Darby canine kidney; MR, mineralocorticoid receptor; mTORC1, mammalian target of rapamycin complex-1; NCC, Na/Cl co-transporter; PC1/2, polycystin-1/2; PDGF, platelet-derived growth factor; RAS, renin-angiotensin system; Wnt, wingless-related integration site.

# 1 | INTRODUCTION

Primary cilia are solitary antenna-like organelles, which protrude from the cell surface of all kidney epithelial cells types except for collecting duct (CD) intercalated cells.[1,2] The structure comprises a microtubule-based axoneme covered by a specialized plasma membrane. The construction and growth of the cilia proceed via intraflagellar transport (IFT), a process of movement of IFT complexes A and B (IFTA and IFTB) associated with retrograde and anterograde transport of tubulin and cargo, along the outer doublet microtubules, respectively.[2,3] The assembly/disassembly of these complexes at the ciliary base as well as their availability and degradation, are crucial factors influencing elongation of primary cilia.[4,5] Primary cilia are thought to be key coordinators of cellular signaling pathways in the regulation of organismal development and tissue homeostasis, such as the sonic hedgehog, wingless-related integration site (Wnt) and platelet-derived growth factor (PDGF)-alpha signaling pathways.[6] In kidney tubules where primary cilia project into the lumen, these organelles may function as fluid flow sensors via calcium entry, which is mediated, at least in part, by the polycystin complex in the ciliary membrane.[7] Defects in the primary cilia are associated with a variety of disorders commonly known as ciliopathies, that exhibit the common feature of kidney cysts.[8,9] These pathologies include mutations of polycystin-1 (PC-1) and polycystin-2 (PC-2), which cause autosomal dominant polycystic kidney disease (ADPKD), one of the most common genetic diseases, and fibrocystin which are implicated in autosomal recessive polycystic kidney disease (ARPKD).[8,10]

The major functions of the kidney are body fluid homeostasis, acid-base balance, clearance of xenobiotics, and metabolic waste products from the blood, and production and/or activation of hormones.[11] Sodium ($Na^+$) is the key determinant of body fluid volume homeostasis and relies on tightly controlled tubular reabsorption of $Na^+$ and water after filtration through the glomeruli. The aldosterone-sensitive distal nephron (ASDN) includes the distal convoluted tubule (DCT) and the collecting system comprising the connecting tubule (CNT) and the CD. The ASDN reabsorbs less than 10% of the filtered $Na^+$ load, which is achieved via Na/Cl co-transporters (NCCs) along the DCT and epithelial $Na^+$ channels (ENaC) along the late DCT, CNT, and CD. This reabsorption is responsible for the fine-tuning of $Na^+$ balance.[11,12] The ASDN is responsive to several hormones including aldosterone, which is secreted by the glomerular zone of the adrenal gland cortex in response to stimulation of the renin–angiotensin system or increased plasma $K^+$ concentration. Aldosterone binds to the cytosolic mineralocorticoid receptor (MR), which then translocates to the nucleus to bind specific DNA sequences and initiate a transcriptional program, which results in stimulation of $Na^+$ reabsorption. In CNT and CD principal cells, aldosterone upregulates the cell surface expression of the ENaCs and the basolateral sodium-potassium-adenosine triphosphatase (Na-K-ATPase), leading to increased transepithelial $Na^+$ reabsorption.[11] Chronic aldosterone stimulation induces principal cell hypertrophy, which increases the $Na^+$ reabsorption capacity of the collecting system.[13]

There has been some experimental evidence that suggests a connection between primary cilia and the sodium transport by CD cells. Drug-induced removal of primary cilia abolishes fluid flow-induced calcium signaling in Madin Darby Canine Kidney (MDCK) cells[14] as well as the flow dependency of $Na^+$ reabsorption in rabbit cortical CD is almost abolished.[15] In CD principal cells, lengthening of the cilia is correlated with decreased intracellular calcium entry, elevated intracellular cyclic adenosine monophosphate (cAMP) levels, and activation of protein kinase A.[16] These two conditions stimulate transepithelial $Na^+$ transport. However, ENaC mediated $Na^+$ absorption has been shown to be increased in cultured CD cells from *orpk* mice (expressing a mutation in Tg737, which encodes the ciliary Polaris protein).[17] In addition, the primary cilia have been shown to control cell volume,[18,19] thus determining the plasma membrane surface that is involved in the exchange between the intracellular and extracellular media. We hypothesized that, in mature renal epithelial cells, primary cilia are structurally dynamic chemosensory organelles, which interact with the $Na^+$ transport system to control cell size. In this study, we show that transepithelial $Na^+$ transport modulates the length of primary cilia by modifying the availability of IFT88 and cell size in a cilium-dependent manner. This functional connection between $Na^+$ transport, primary cilia, and cell size may play a key role in the morphological and functional adaptation of the CD to sustained changes in active $Na^+$ reabsorption in response to variations in aldosterone secretion.

# 2 | MATERIALS AND METHODS

## 2.1 | Antibodies and chemicals

Antibodies are listed in Table 1, respectively. Benzamil (B2417), aldosterone (A9477-5MG), and bafilomycin (B1793) were from Sigma-Aldrich (St. Louis, MO, USA).

## 2.2 | Animals

The previously described doxycycline-inducible kidney tubule-specific[20] and mosaic[21] MR-deficient mice were used for experiments. Kidney tubule-specific MR knockout (KO) induced by administration of doxycycline hydrochloride (2 mg/mL in drinking water) for 15 days to 4-week-old mice.

**TABLE 1** Antibodies

| Title | Catalogue number | Dilution used | Company |
|---|---|---|---|
| *Primary antibodies* | | | |
| Acetylated tubulin | T6793 | WB: 1/2000, IF: 1/500 | Sigma, St. Louis, MO |
| Atg12 | 2011S | WB: 1/1000, IF: 1/500 | Cell Signaling Technology, USA |
| Beta actin | A5441 | 1/10000 | Sigma, St. Louis, MO |
| E-cadherin | 610181 | WB :1/2000 | BD Transduction Laboratories |
| GAPDH | MAB374 | 1/20000 | Millipore |
| IFT88 | 13967-1-AP | WB: 1/1000 | Proteintech, Rosemont, IL |
| LC3B | L7543 | IF: 1/500 | Sigma, St. Louis, MO |
| p62 (SQSTM1) | ab56416 | WB :1/1000 | Abcam, Cambridge, UK |
| p70 S6 kinase | 9202 | WB: 1/1000 | Cell Signaling Technology, USA |
| P-p70 S6 kinase | 9234S | WB: 1/1000 | Cell Signaling Technology, USA |
| SGK | S5188 | WB :1/2000 | Sigma, St. Louis, MO |
| *Secondary antibodies* | | | |
| Alexa Fluor 488-conjugated goat anti-mouse | cat. no. A-11017 | IF 1:500 | Invitrogen, CA, USA |
| Ga α-mouse HRP | | 1:20000 | BD Biosciences Pharmingen |
| Ga α-rabbit HRP | | 1:20000 | BD Biosciences Pharmingen |

Triple transgenic mice (with two floxed alleles of MR, reverse tetracyclin transactivator under the control of the Pax8 promoter and Cre recombinase under the control of a tetracycline responsive element) resulting in targeted expression of Cre recombinase in renal tubular cells and Nr3c2 deletion. Mosaic MR (KO) mice are double transgenic mice carrying carries two floxed alleles of MR and X chromosome linked Cre recombinase under the control of a Cytomegalovirus (CMV) promoter. In this setting, Cre transcription is regulated by mechanisms of X chromosome dosage compensation in females. MR/X female mice were carrying MR deletion in 20% of ASDN cells.

## 2.3 | Cell culture

Mouse cortical collecting $duct_{c11}$ cells, a well-characterized mouse CD principal cell line,[22] were seeded at a density of 200 000 cells per filter and grown on polycarbonate filters (Transwell, Corning-Costar, Cambridge, MA, USA) for 4 days until 100% confluency in "growth medium" containing DMEM-F12 (Invitrogen-GIBCO), 5 μg/mL insulin (Sigma), 5 μg/mL holo-transferrin (Sigma), 2% FCS (Invitrogen-GIBCO, Carlsbad, CA, USA) 10 ng/mL EGF (PeproTech, Rocky Hill, NJ, USA), 50 nM dexamethasone (Sigma), 60 nM sodium selenite (Sigma), and 1 nM 3,3′,5-triiodo-L-thyronin (Sigma). For experiments, we used filters displaying at least 2000 Ohm and 2-10 mV transepithelial resistance and voltage, respectively. Under this condition cells do not display well developed cilia at day 4. To induce ciliogenesis, *cells are grown* in "starvation medium" containing serum and hormone-deprived DMEM/F12 (Invitrogen-GIBCO) supplemented with 5 μg/mL holo-transferrin (Sigma) and 60 nM sodium selenite (Sigma). Aldosterone was added at the same time as starvation started. Experiments with either 0 or 150 mM apical $Na^+$ were performed in the presence of starvation medium in the basal chamber and a defined medium in

the apical chamber which contained (in mM) 0.3 $MgCl_2$, 0.4 $MgSO_4$, 14.3 $KHCO_3$, and 0.5 $K_2HPO_4$ supplemented with either 150 mM choline chloride to keep osmolality constant for the 0 $Na^+$ condition or 150 mM NaCl for the 150 $Na^+$ condition. Measurement of electrical parameters, sample fixation for the immunofluorescence or protein extraction were done sequentially at day 5 (24 hours after a treatment/starvation started).

For experiments, we used previously described stably transfected/transduced $mCCD_{cl1}$ cells which display doxycycline-inducible γ-ENaC subunit overexpression[23] or doxycycline-inducible IFT88 silencing[24] obtained after transduction with a pTRIPZ lentiviral construct (Snapgene, Chicago, Il, USA) or $mCCD_{cl1}$ cells with constitutive silencing of γ-ENaC subunit or overexpression of IFT88 obtained after transduction with pLKO (Sigma) or PSF (Addgene, Watertown, MA, USA) lentiviral constructs, respectively.

## 2.4 | Transepithelial resistance and potential difference measurement

The values of transepithelial resistance and potential difference were measured with a Millicell-ERS ohm-volt meter (Millipore, Billerica, MA, USA) before protein extraction or cell fixation.

## 2.5 | Cell lysates and Western blotting

Cells were lysed in homogenizing buffer containing (in mM) 20 Tris, pH 7.4, 2 EGTA, 2 EDTA, 30 NaF, 30 $Na_4P_2O_7$, and 2 $Na_3VO_4$ supplemented with 0.1% SDS, 1% Triton-X100, and a protease inhibitor cocktail (Complete Mini, Roche, Mannheim, Germany). Equal amounts of protein (15 μg) were separated by SDS-PAGE (8% or 12% polyacrylamide) and transferred to polyvinylidene difluoride membranes (Immobilion-P, Millipore). After incubation with primary antibodies (Table 1), membranes were incubated with anti-rabbit or anti-mouse IgG antibody coupled to horseradish peroxidase (Transduction laboratories, Lexington, KY), the antigen antibody complexes were detected by enhanced chemiluminescence (Advansta, Menlo Park, CA). Protein abundance was quantified with the image J software. Results are expressed as the ratio of the densitometry of the band of interest to the loading control.

## 2.6 | Real-time PCR

Total RNA from cultured cells was extracted using the EZNA Total RNA Kit I (Promega, Madison, WI, USA) according to the manufacturer's instructions. RNA concentration and purity was measured using Nanodrop. One μg of RNA was used to synthesize cDNA using qScriptTM Reverse Transcriptase (Quanta Biosciences, Gaithersburg, MD) according to the manufacturer's instructions. Primers for IFT88 were 5′-TGAGGACGACCTTTACTCTGG-3′ and 3′-CTGCCATGACTGGTTCTCACT-5′ and for P0 ribosomal protein were 5′-AATCTCCAGAGGCACCATTG-3′ and 3′-GTTCAGCATGTTCAGCAGTG-5′. PCR was performed on 3 μL of cDNA diluted 1:10 (v/v) using 0.5 μM of each primer and 7 μL of SYBR Green Master Mix (Applied Biosystems; Foster City, CA, USA) to obtain a final reaction volume of 14 μL. Duplicate amplification reactions were performed with an ABI StepOne sequence detection system (Applied Biosystems). Data were analyzed using the ABI Prism software (Applied Biosystems) and P0 was used as an internal standard. Fold difference in cDNA abundance (F) was calculated using the formula $F = 2^{(Ct1-Ct2)}$ where Ct1 and Ct2 are the number of cycles required to reach the threshold of amplicon abundance for experimental and control conditions, respectively.

## 2.7 | Immunofluorescence

Kidneys were removed after fixation by perfusion with 4% paraformaldehyde, dehydrated, and paraffin-embedded. Kidney sections of 10 μm thickness were used for analysis. For immunofluorescence, slides were counterstained with DAPI for the nuclei staining. Immunofluorescence analysis on kidney sections was performed as described previously.[21] Confocal imaging and z-stacks were performed on a Nikon A1R confocal microscope, objective 60 × 1.4 CFI Plan Apo Lambda WD: 0.13 mm. A total amount of 25-30 Z-slices were imaged to make sure that the entire primary cilia are measured. Distance between the Z-slices was 0.25 μm. From 5 to 10 Z-stack images (images that contain fluorescent staining) were summarized, and primary cilium length was measured using the ImageJ software (National Institute of Health, Bethesda, MD, USA).

Cells grown to confluence on polycarbonate filters were fixed (together with filters) with ice-cold methanol for 2 minutes at −20°C and then washed with PBS. After washing for 30 minutes, blocking of nonspecific binding sites was done with PBS containing 2% bovine serum albumin (PBS-BSA) at room temperature (RT). Finally, cells were incubated overnight at 4°C with antibodies against acetylated α-tubulin diluted in 0.2% PBS-BSA followed by 1 hour incubation with Alexa Fluor 488-conjugated goat anti-mouse (cat. no. A-11017; Invitrogen) diluted 1:500 in PBS-BSA. Samples were mounted on microscope slides using Vectashield mounting medium (Maravai Life Science, San Diego, CA, USA) with DAPI for nuclear counterstaining. Fluorescence images were acquired using a LSM 710 confocal laser-scanning

microscope (Carl Zeiss, Oberkochen, Germany) using 488-nm and 561-nm ray lasers. Distance between the Z-slices was 0.25 μm. From 5 to 10 Z-stack images were summarized, and primary cilium length was measured using the ImageJ software (National institute of Health, Bethesda, MD, USA).

## 2.8 | STED nanoscopy

Cells grown on 12-mm glass coverslips were fixed with ice-cold methanol for 2 minutes at −20°C and then washed with PBS. After washing for 30 minutes, blocking of nonspecific binding sites was done with PBS containing 2% bovine serum albumin (PBS-BSA) at room temperature (RT). Finally, cells were incubated overnight at 4°C with antibodies against acetylated α-tubulin diluted in 0.2% PBS-BSA followed by 1 hour incubation with a goat anti-mouse STAR RED secondary antibody (Abberior GmbH, Göttingen, Germany) diluted 1:1000 in PBS-BSA. Samples were mounted in ProLong Gold antifade medium (ThermoFisher scientific) on microscope slides with 1.5 coverslips (0.170 ± 0.01 mm, Hecht-Assistant, GmbH) sealed with nail polish.

The samples were placed on a Leica TCS SP8 STED 3X inverted microscope, which was temperature controlled to 21 C, to avoid drift throughout the image acquisition and to ensure refractive index match between the glass slide, cells, and immersion medium. Images were acquired using a Leica HC PL APO CS2 100×/1.40 oil objective.

A white light laser fully tunable in the range of 470-670 nm was used to excite precisely the fluorophore to the nearest nm (Leica SuperK extreme, Wetzlar, Germany).

STAR RED labelling was imaged using 638-nm excitation laser line and 775-nm STED pulsed depletion laser. The detection range was from 650 to 720 nm. Gating was from 0.5 to 5 ns; no line averaging and accumulation were performed. The fluorescent signal was collected with a Leica hybrid detector (HyD). Images were automatically deconvoluted after acquisition using the Lightning mode available in the Leica LAS X software.

## 2.9 | Cell volume measurement

Cells were grown on fluorodishes (WPI, FD35-100) until they are confluent and then treated or not with aldosterone for 24 hours. Afterward cells were labelled with plasma membrane stain (ThermoFisherScientific, C10046). Fluorescence images were acquired using a Nikon A1R confocal microscope, objective 60 × 1.4 CFI Plan Apo Lambda WD: 0.13 mm, 60× magnification. A total amount of 25-30 Z-slices were imaged to make sure that the entire primary cilia are measured. Distance between the Z-slices was 0.3 μm. Cell volume was extracted from Z-stack images using Amira software (the Amira script is available upon request). To validate the method, we immersed in the same image Amira reconstructed 3D image with original Z-stack file to see the confocal image/model overlap (Figure S7A, Video 1). Areas where several individual cells were merged together during volume extraction were not included in analysis.

Z-stack images were first filtered using a nonlocal means filter (Search and local neighborhood windows [21 5], similarity at 0.6) followed by a linear stretched of the contrast. The Far-red membrane staining negative parts of the images were segmented using an H-minimum transform (contrast of 100), as a result the outer cell layer and the cytosolic part of the cells were labelled. The outer cell layer was discarded as this is the biggest volume of all the segmented elements. The remaining cytosolic objects were eroded by a ball, in order to separate the potential contacts between cytosols of adjacent cells. These were used as the markers of a constrained watershed segmentation, where the intensity image was directly normalized one after the nonlocal means filter. Indeed, the membrane labelling can be assimilated to the gradient given by a cytosolic labelling. Such a procedure allowed to reconstruct cells in contact individually and in 3D. Consequently, the volume of each cell was computed and color coded for graphical representation.

## 2.10 | Statistical analyses

Results are given as mean ± SEM or SD (cilium length) from three to five independent experiments. Statistical analysis was done using GraphPad Prism software. Comparison of potential difference, primary cilium length and cell volume values we performed using two-tailed unpaired *t* test for two groups and one-way ANOVA for more than two groups. Comparison of Western blot quantifications were performed by Mann-Whitney U test for two groups and by Kruskal-Wallis test for more than two groups. $P < .05$ was considered significant.[25]

# 3 | RESULTS

## 3.1 | A cell autonomous mechanism controls the length of primary cilia through a mineralocorticoid receptor-dependent pathway

Inducible kidney tubule-specific MR KO (tubular MR KO) mice display a severe pseudohypoaldosteronism type 1 phenotype characterized by weight loss, increased urinary $Na^+$ excretion, hyponatremia, hyperkalemia, and high plasma aldosterone levels.[20] This phenotype is attributed to decreased $Na^+$ reabsorption and $K^+$ secretion along the ASDN. To investigate whether MR directly or indirectly controls primary cilium length, we measured the length of cilia along the

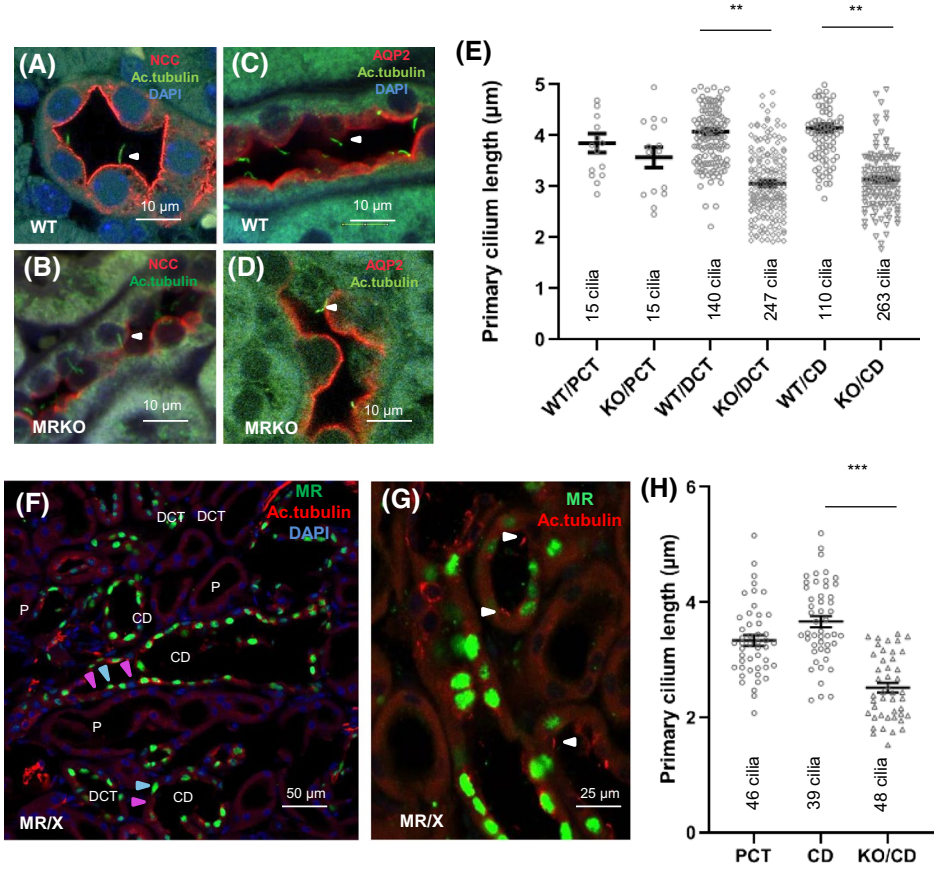


**FIGURE 1** Primary cilium length is controlled by a cell autonomous mechanism involving a mineralocorticoid receptor-dependent pathway. A-E, Doxycycline-inducible and kidney tubule-specific mineralocorticoid receptor knockout (MR KO) mice exhibited shorter primary cilia along the aldosterone-sensitive distal nephron (ADSN) including the distal convoluted tubule (DCT) and collecting duct (CD). Two weeks after MR KO in kidney tubular cells with doxycycline treatment, kidney sections of wild-type (WT) and KO mice were co-stained with antibodies against (A and B) Na/Cl co-transporter (NCC) for DCT, (C and D) aquaporin-2 (AQP2) for CD, and acetylated α-tubulin for primary cilia (indicated with white arrows). Primary cilium length was measured on z-stacks using ImageJ software (National Institute of Health, US). Four or five animals were analyzed for each condition (WT or KO). E, Individual measurements (circles) and mean ciliary length (lines) as well as standard error bars are shown. The number of measured cilia is indicated on the upper part of the graph. F-H, Cilia length of MR KO CD principal cells is decreased compared with that of WT CD principal cells and proximal tubule cells. Kidney sections from female mosaic MR KO mice were co-stained with antibodies for MR and acetylated α-tubulin for primary cilia. Cells expressing MR exhibited nuclear staining (blue arrow), which was absent in MR KO cells (pink arrow). Primary cilia are indicated by white arrows in panels F and G. Mean primary cilia length from data of three animals was measured from z-stacks using ImageJ software (National Institute of Health, US). Individual measurements (circles) and mean cilia length (lines) as well as standard error bars are shown in panel H. The number of measured cilia is indicated in the upper part of the graph

ASDN in tubular MR KO mice and wild-type (WT) control littermates. Primary cilia were stained with antibodies against acetylated α-tubulin, while DCT and CNT/CD were visualized using apical NCC and aquaporin-2 (AQP2) staining, respectively. Proximal convoluted tubule (PCT) cells were identified by morphology and the presence of a brush border. Owing to the presence of the brush border, it was difficult to image primary cilia in PCT; therefore, only a few cilia could be measured. We observed shorter primary cilia in both DCT (as μm ± SEM: WT, 3 ± 0.1; KO, 3.12 ± 0.13) and CNT/CD cells (as μm ± SEM: WT, 4 ± 0.11; KO, 3.17 ± 0.15) of MR KO mice but cilium length was unaltered in the PCT cells (as μm ± SEM: WT, 3.9 ± 0.2; KO, 3.8 ± 0.04) of MR KO mice compared to control WT mice (Figure 1A-E).

To determine whether the observed MR KO-dependent ciliary shortening was "cell autonomous" or relied on a local or systemic extracellular signal, we analyzed mice with randomized MR deletions (MR/X mice). In MR/X mice, MR-positive (80%), and MR KO (20%) cells coexist along the same tubule and in the same physiological context.[21] We did not detect any changes in renal $Na^+$ and $K^+$ homeostasis in adult mosaic MR KO mice (MR/X) fed a normal salt diet. However, when MR/X mice were challenged for 2 days with dietary $Na^+$ restriction (0.03% $Na^+$), increased urinary $Na^+$ excretion and 24 hours urinary aldosterone were observed, while urinary $K^+$ excretion was decreased.[21] We measured ciliary length in CD principal cells, which expressed or did not express MR, and in proximal tubule cells, which were considered as a control in three

different animals. It is worth mentioning that intercalated cells do not display primary cilia. We found cilia to be shorter in MR KO principal cells compared with principal cells expressing MR (2.35 ± 0.3 μm vs 3.8 ± 0.5) (Figure 1F-H). Ciliary length was similar for PCT cells and WT principal cells (Figure 1H). These results suggest that MR-dependent regulation of ciliary length is dependent on cell autonomous mechanism.

### 3.2 | Aldosterone caused primary cilia to lengthen in cultured collecting duct principal cells

Experiments showing that MR KO decreases primary cilium length in physiologically aldosterone-responsive cells led us to assess the effect of aldosterone on primary cilium length in cultured aldosterone-responsive cells. The mouse CD cell lines $mCCD_{cl1}$ and $mpkCCD_{cl4}$ cells[22,26] exhibit the major features of native principal CD cells such as responsiveness to aldosterone and vasopressin.

We treated $mCCD_{cl1}$ cells for 24 hours with $10^{-6}$ M aldosterone (maximal effective concentration to achieve potential difference response) in starvation media before measurement of transepithelial resistance and potential followed by staining of the primary cilia and immunofluorescence analysis. To ensure fixation with ice-cold methanol did not damage the organelles, we performed stimulated emission-depleted (STED) nanoimaging of 10 random primary cilia and basal bodies, which appear as dots on confocal images (Figure S1A-D). The primary cilia were found to be located in the middle of the apical membrane, attached to a basal body and with decreasing thickness that decreases from the base to the tip. Evidence for traumatic shortening was not noticed among the analyzed cilia (Figure S1A-B). Non-ciliated cells exhibited two centrioles, either separated (Figure S1C) or together, with the morphology of a basal body (Figure S1D).

Aldosterone-treated cells displayed increased transepithelial potential difference, reflecting increased vectorial $Na^+$ transport, from the apical to the basal pole of the filter (Figure 2A) and longer primary cilia were observed, as illustrated by the violin plot (Figure 2B). The objects and information shown in the violin plots are presented in Figure S1E. Aldosterone-induced ciliary lengthening (from 2.7 ± 0.9 to 3.8 ± 0.8 μm) was also observed in $mpkCCD_{c14}$ cells (data not shown).

To test whether ciliary lengthening in response to aldosterone relies on MR activation, we treated cells with $10^{-5}$ M 17-hydroxyprogesterone (17-OHP), a specific MR antagonist.[27] Treatment of the renal CD cells with $10^{-5}$ M 17-OHP alone had no effect on the length of cilia, but prevented the stimulatory effects of aldosterone on both transepithelial potential difference and primary cilium growth (Figure 2E,F). Taken together, these results indicate that aldosterone modulates the primary cilia length via MR signaling in cultured CD principal cells.

To assess whether aldosterone also controls the length of primary cilia when administered at low physiological concentrations, we performed a dose-response experiment using aldosterone concentrations of 3-100 nM for 12 hours. A statistically significant increase in transepithelial potential difference and length of cilia was observed following exposure to aldosterone concentrations of 30 nM or higher (Figure S2A,B). This indicates that aldosterone would induce this effect when present in nM concentrations (which reflects the physiological concentration range). Time-course experiments showed that the cilia lengthening as well as the increase in transepithelial potential difference was significant after 2 hours exposure to 1 μm aldosterone (Figure S2C,D).

### 3.3 | Transepithelial $Na^+$ influx modulates the length of cilia in cultured collecting duct principal cells

To investigate the effect of transepithelial $Na^+$ influx on the length of primary cilia, we challenged $mCCD_{cl1}$ cells for 24 hours with two different apical $Na^+$ concentrations (0 and 150 mM), while maintaining basal $Na^+$ at ~140 mM (see Section 2, Cell culture). Under these conditions, we compared cells displaying low (0 $Na^+$) and high (150 $Na^+$) intensity transepithelial $Na^+$ transport without using any chemical or hormone-dependent effect. The transepithelial potential difference was lower in cells that were incubated with 0 mM than with 150 mM apical $Na^+$, as expected (Figure 3A). Cells incubated with 0 mM apical $Na^+$ mostly displayed centrioles; and a few 1.5 ± 0.5 μm in length exhibited a positive result after staining with anti-acetylated α-tubulin antibodies. In contrast, 150 mM apical $Na^+$ resulted in well-developed primary cilia that were 2.6 ± 0.4 μm long (Figure 3B-D). Taken together with our results of the effect of aldosterone, primary cilium growth appears to be linked to the intensity of transepithelial $Na^+$ transport.

To confirm the role of $Na^+$ transport in the control of ciliary lengthening, we assessed the role of ENaC-dependent $Na^+$ entry in the modulation of this parameter. We first assessed the effect of knockdown of the rate limiting γ-ENaC subunit.[23] Silencing γ-ENaC subunit expression with shRNA caused a significant decrease in transepithelial voltage and the length of the primary cilia decreased from 3.6 ± 0.3 μm to 0.1 ± 0.03 μm to (Figure 3E-I). Treatment of $mCCD_{cl1}$ cells with $10^{-6}$ M benzamil, a specific ENaC blocker, resulted in cilia shortening under control conditions (control: 3 ± 0.1 μm and benzamil treated: 2.9 ± 0.1 μm) and abrogated the effects of aldosterone on both transepithelial potential difference and ciliary length (aldosterone treated: 3 ± 0.4 μm and and aldosterone/benzamil treated: 2.7 ± 0.2 μm) (Figure 4A,B). These results indicate that the length of primary cilia is linked to ENaC-dependent transepithelial $Na^+$ transport in CD principal cells.

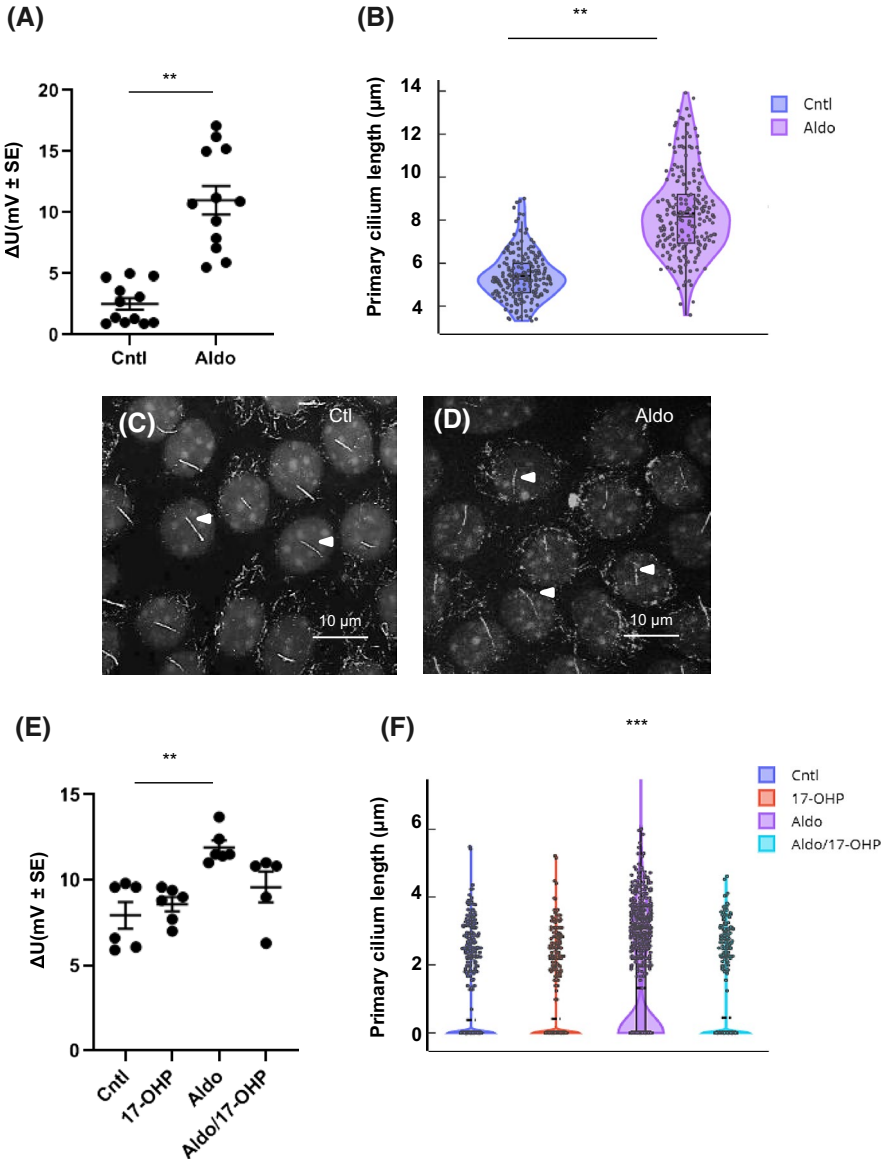


**FIGURE 2** Aldosterone stimulation of vectorial sodium transport is associated with increased cilia length, which relies on mineralocorticoid receptor signaling in collecting duct principal cells. We grew $mCCD_{cl1}$ cells to confluence on polycarbonate filters. Cells were incubated in the absence or presence of $10^{-6}$ M aldosterone for 24 hours. A, Transepithelial potential difference measured in 12 filters. Each point represents a single measurement and bars represent the mean ± standard error of the mean. B-D, Cells were fixed and stained with antibodies against acetylated α-tubulin to visualize primary cilia. B, Violin plot showing repartition of primary cilia by length with 350-400 cilia per condition. Each point represents data of a single cilium and bars represent the means ± standard deviation. C and D, Representative z-stack images of six independent experiments. E and F, Cells were pre-incubated for 1 hour in the absence or presence of $10^{-5}$ M 17-hydroxy-progesterone (17-OHP) followed by addition of $10^{-6}$ M aldosterone (Aldo) for an additional 24 hours. E, Transepithelial potential difference measured in six filters. Each point represents a single measurement and error bars represent the mean ± standard error of the mean. F, Violin plot showing repartition of primary cilia by length with 800-1100 cilia per condition. Results are from three independent experiments. Points represent the length of a single cilia and bars represent the mean ± standard deviation. Statistical analysis was performed by two-tailed Student's *t* test for unpaired data to compare two groups and one-way analysis of variance to compare more than two groups. $^{**}P < .01$

## 3.4 | Aldosterone upregulates mammalian target of rapamycin complex 1 in cultured collecting duct principal cells

The mammalian target of rapamycin complex-1 (mTORC1) was recently identified as a regulator of renal $Na^+$ and $K^+$ handling, and has been reported to be involved in the control of cilium growth.[18,28,29] We therefore assessed the effects of aldosterone of mTORC1 activation. Exposure of $mCCD_{cl1}$ cells to $10^{-6}$ M aldosterone for 1-6 hours caused increased phosphorylation of p70-RSK, the downstream target of mTORC1 (Figure 5A). Similarly, phosphorylation of p70-RSK was higher in $mCCD_{cl1}$ cells incubated with

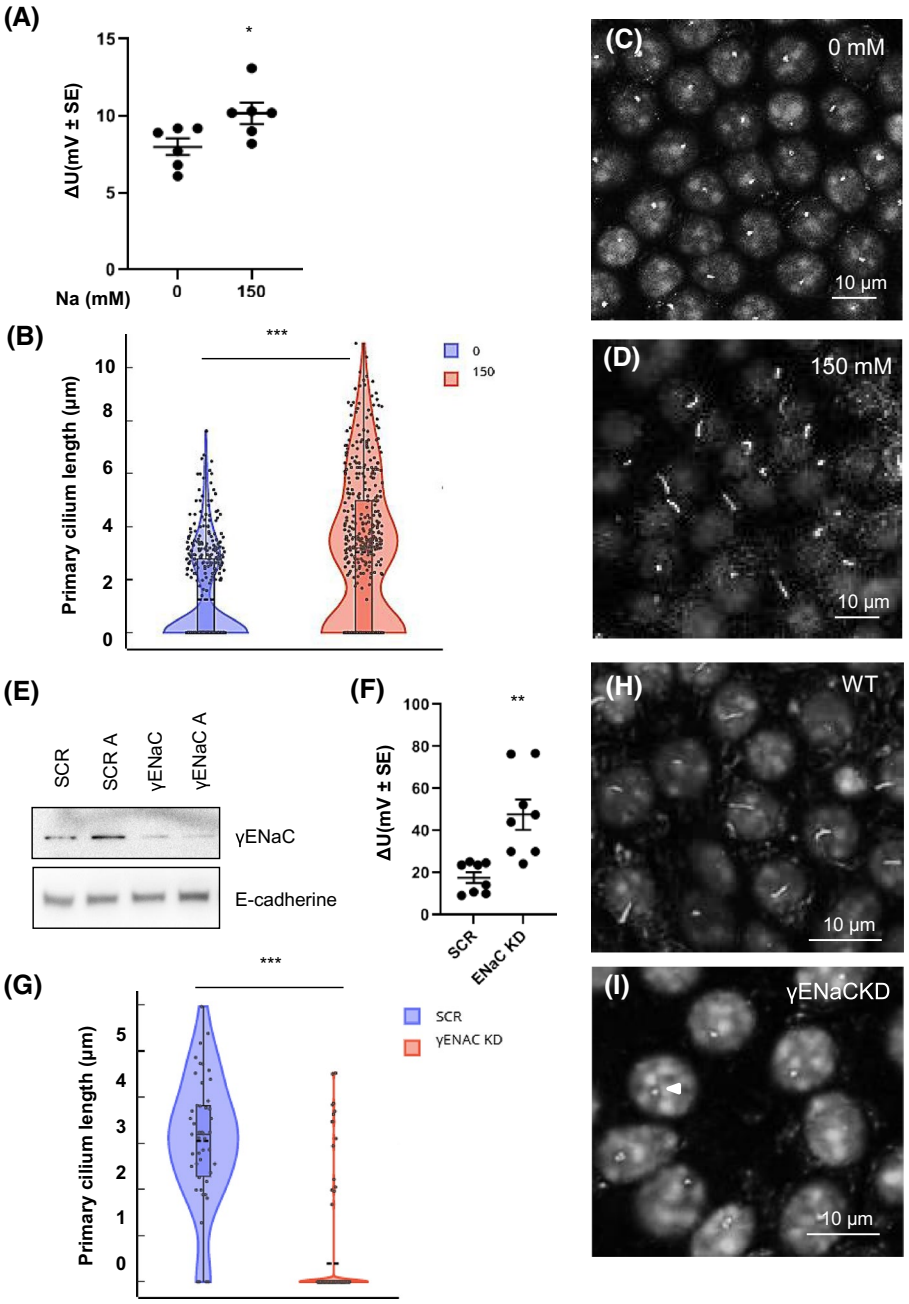


**FIGURE 3** $Na^+$ influx modulates cilia length in collecting duct principal cells. Confluent $mCCD_{cl1}$ cells were grown to confluence on polycarbonate filters. Cells were incubated with either 0 or 150 mM apical $Na^+$ for 24 hours. Osmolality was kept constant by the addition of 150 mM choline chloride, which substituted NaCl in the $Na^+$-free medium. A, Transepithelial potential difference measured in six filters. Each point represents a single measurement and bars represent mean ± standard error of the mean. B, Violin plot showing repartition of primary cilia by length with 300-400 cilia per condition. Results are from four independent experiments. Points represent the length of a single cilia and bars represent mean ± standard deviation. C and D, Representative summarized z-stack images of four independent experiments. E-I, After transduction with lentivirus encoding either scrambled shRNA (WT) or shRNA targeting γ-epithelial sodium channels (ENaC; ENaC-KD), $mCCD_{cl1}$ cells were grown to confluence on polycarbonate filters. E, Representative western blot of three experiments demonstrating γ-ENaC silencing. F, Transepithelial potential difference measured in eight filters. Each point represents a single measurement and bars represent mean ± standard error of the mean. G, Violin plot showing repartition of primary cilia by length with 130-150 cilia per condition. Results are from four independent experiments. Points represent the length of a single cilia and bars represent mean ± standard deviation. H and I, Representative summarized z-stack images of four independent experiments. Statistical analysis was performed by two-tailed Student's *t* test for unpaired data to compare two groups and one-way analysis of variance to compare more than two groups. $*P < .05$

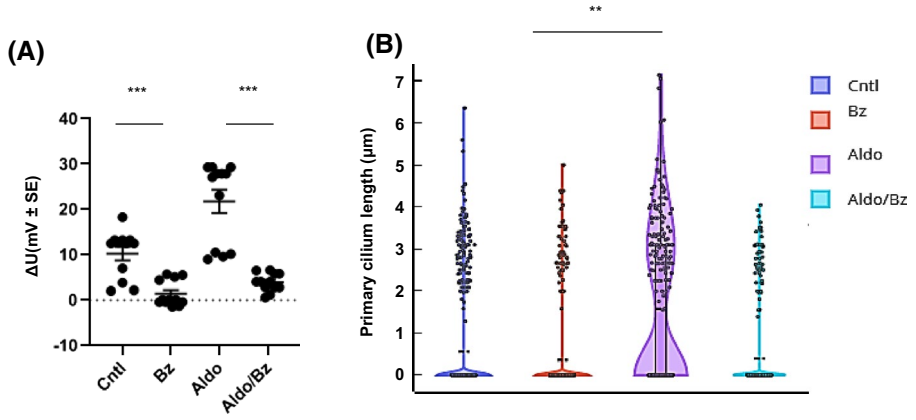


**FIGURE 4** Elongation of primary cilia in response to aldosterone is inhibited by benzamil, a specific ENaC inhibitor. Cells were pre-incubated in the presence or absence $10^{-6}$ M benzamil (Bz) for 1 hour before the addition of $10^{-6}$ M aldosterone (Aldo) for an additional 24 hours. A, Transepithelial potential difference measured in six filters. Each point represents a single measurement and bars represent mean ± standard error of the mean. B-E, Representative summarized z-stack images of four independent experiments. F, Violin plot showing repartition of primary cilia by length with 300-400 cilia per condition. Results are from four independent experiments. Points represent the length of a single cilia and bars represent mean ± standard deviation. Statistical analysis was performed by one-way analysis of variance. *$P < .05$

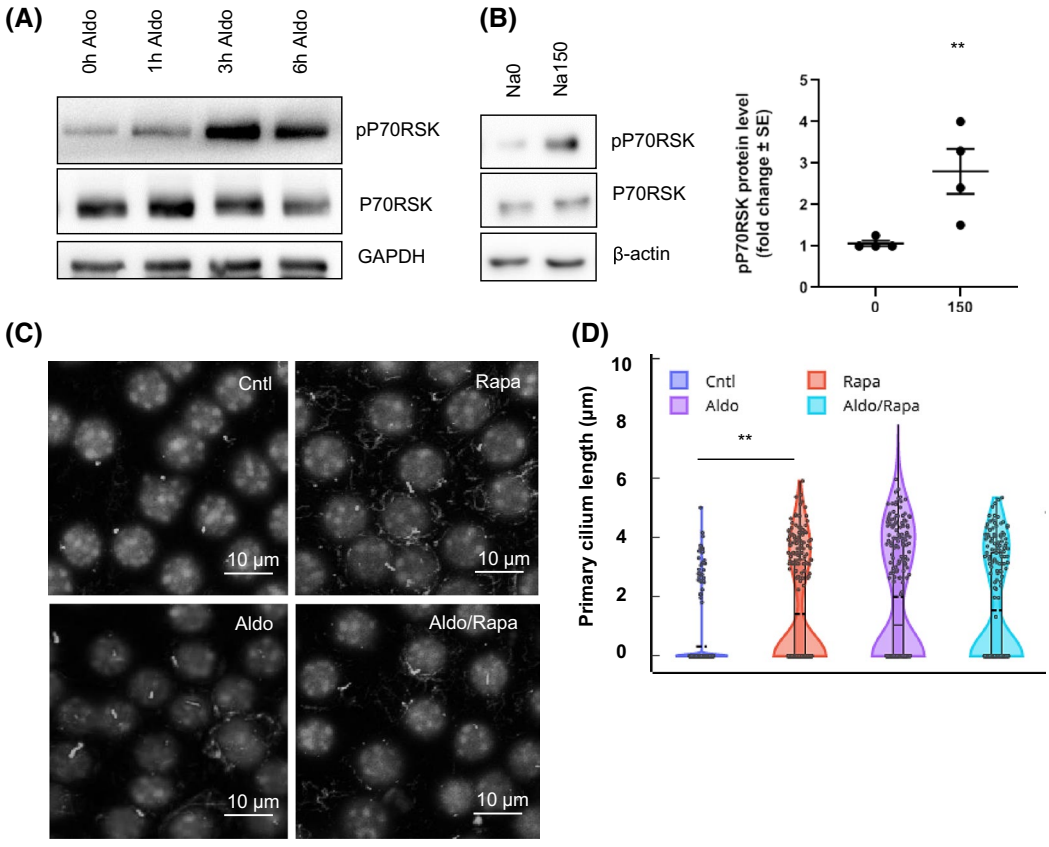


**FIGURE 5** Aldosterone induces activation of mammalian target of rapamycin complex-1 in collecting duct principal cells. Confluent $mCCD_{cl1}$ cells grown on polycarbonate filters were incubated for 9 hours in serum- and hormone-deprived medium in the absence (0 hours Aldo) or presence of $10^{-6}$ M aldosterone (Aldo) for 1, 3, or 6 hours. A and B, Representative western blot from four independent experiments showing (A) increased phosphorylation of p70RSK in response to aldosterone and (B) in the presence of 150 mM apical $Na^+$ for 24 hours. Beta-actin served as a loading control. C, Representative summarized z-stack images of four independent experiments. D, Violin plot showing repartition of primary cilia by length with 200-220 cilia per condition. Results are from four independent experiments. Points represent the length of a single cilia and bars represent mean ± standard deviation. Statistical analysis was performed by one-way analysis of variance. *$P < .05$

150 mM apical $Na^+$ compared 0 mM apical $Na^+$ (Figure 5B). These results strongly suggest that increased transepithelial transport is associated with stimulation of mTORC1 in CD principal cells.

Inhibition of mTORC1 with $10^{-5}$ M rapamycin caused a slight increase in ciliary length but did not alter aldosterone-induced elongation of cilia (Figure 5C,D). Therefore, stimulation of mTORC1 alone does not explain the increase in length of cilia that we observed in response to increased transepithelial $Na^+$ transport.

### 3.5 | Aldosterone signaling promotes ciliogenesis via decreased IFT88 protein degradation in cultured collecting duct principal cells

To determine whether aldosterone affects ciliary lengthening through its effects on IFT, we investigated protein levels and degradation of the core IFT complex B protein, IFT88 and the molecular motor, KIF3A, which are involved in anterograde transport and ciliary growth, respectively.[34,35]

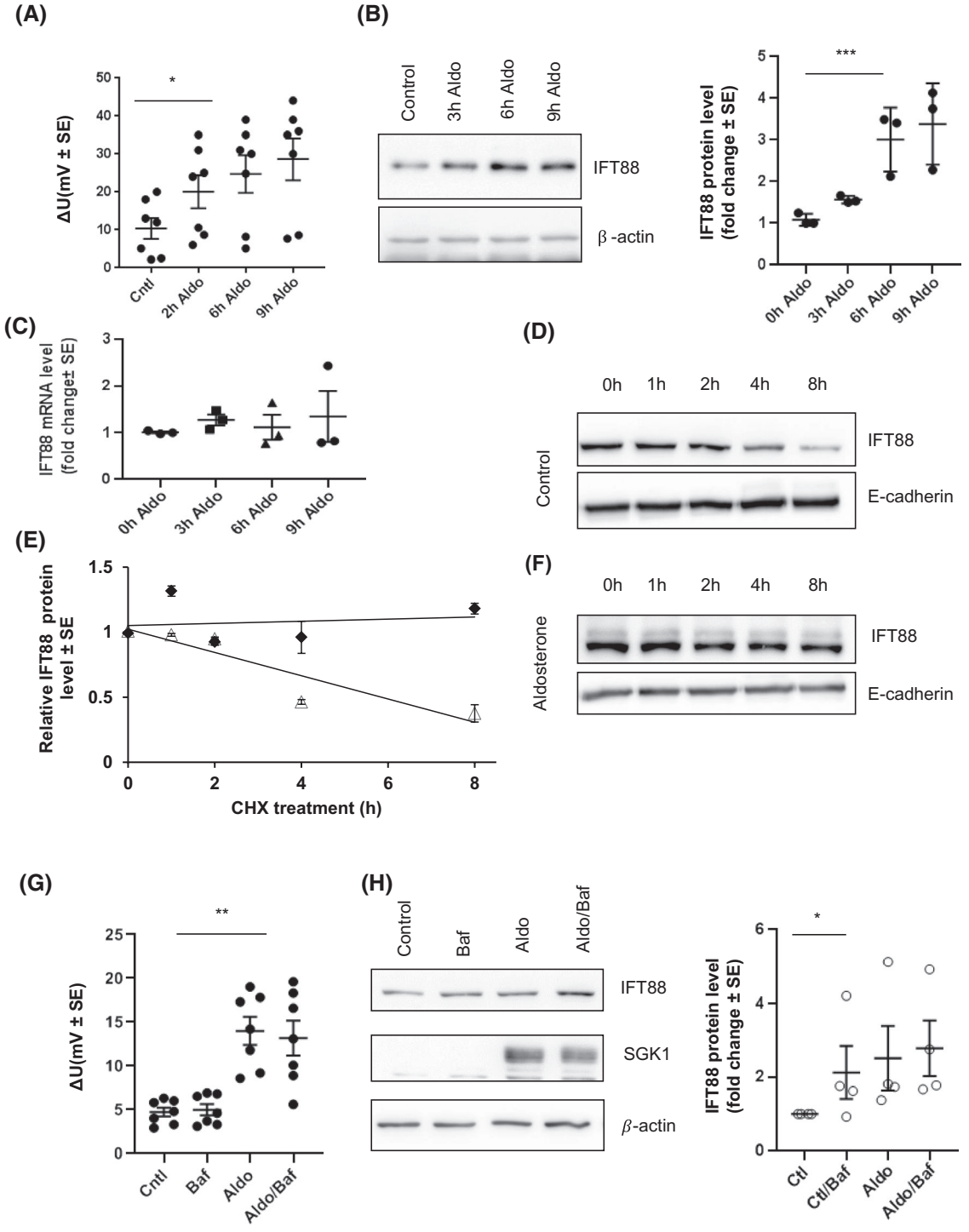

**FIGURE 6** Aldosterone stabilizes IFT88 by inhibiting its degradation in collecting duct principal cells. Confluent $mCCD_{cl1}$ cells grown on polycarbonate filters were incubated in serum- and hormone-deprived medium for 24 hours in the absence (0 hours Aldo) or presence of $10^{-6}$ M aldosterone (Aldo) for 3, 6, or 9 hours. A, Transepithelial potential difference measured in seven filters. Each point represents a single measurement and bars represent mean ± standard error of the mean. B, Representative western blot from three independent experiments with β-actin as a loading control. Abundance of IFT88 increased in response to aldosterone in a time-dependent manner. C, Levels of IFT88 mRNA were not affected by aldosterone according to real-time quantitative polymerase chain reaction. D-F, Cells were pre-incubated for 24 hours in the absence (control) or presence of $10^{-6}$ M aldosterone prior to incubation for 8 hours in the absence (0 hours) or presence of $2.10^{-6}$ M cycloheximide (CHX), which inhibits protein synthesis. D and F, Representative western blots [form] from three independent experiments with E-cadherin as a loading control. E, Western blots were quantified using ImageJ software and results expressed as fold of control ± standard error of the mean. G and H, Confluent $mCCD_{cl1}$ cells grown on polycarbonate filters were incubated for 9 hours in serum- and hormone-deprived medium in the absence (Cntl) or presence of $10^{-6}$ M aldosterone (Aldo) and/or 100 nM bafilomycin, which was added 2 hours before the end of the experiment. G, Transepithelial potential difference measured in six filters. Each point represents a single measurement and bars represent mean ± standard error of the mean. H, Bafilomycin and aldosterone caused the abundance of IFT88 to increase. Serum/glucocorticoid-regulated kinase 1 is shown as a positive control of the biological activity of aldosterone. The left panel shows a representative western blot from four independent experiments. The right panel illustrates quantification of western blots using ImageJ software (National Institute of Health, US). Each point represents a single measurement and bars represent mean ± standard error of the mean. Statistical analysis was performed by one-way analysis of variance. $*P < .05$

Aldosterone treatment increased IFT88 protein abundance and amiloride-sensitive transepithelial potential difference in a time-dependent manner (Figure 6A,B). Because mRNA levels of IFT88 were not altered (Figure 6C), we assessed the protein stability of IFT88 by cycloheximide (CHX) chase assay. Under conditions where protein synthesis was inhibited by CHX, aldosterone treatment prevented IFT88 degradation (Figure 6D-F). Bafilomycin A1, a potent inhibitor of the Vacuolar $H^+$-ATPase (V-ATPase) that prevents lysosomal acidification and inhibits protein degradation, caused a strong increase in both IFT88 abundance and the length of primary cilia from 0.3 ± 0.02 to 1.9 ± 0.5 μm (Figures 6H and S2C). The stimulatory effects of aldosterone and bafilomycin A1 on ciliary lengthening were not additive; bafilomycin A1 altered neither basal nor aldosterone-stimulated $Na^+$ transport (Figure 6G). These results suggest that aldosterone inhibits lysosomal degradation of IFT88.

Because IFT88 protein stability was increased by aldosterone, we investigated the role of IFT88 availability in ciliary lengthening. We analyzed $mCCD_{cl1}$ cells that exhibited doxycycline-inducible silencing (Figure 7A-C) as well as constitutive overexpression (Figure 7D-G) of IFT88. Remarkably, both overexpression and knockdown of IFT88 had no effect on the transepithelial $Na^+$ transport (Figure 7A,D). As described previously,[24] cells with doxycycline-induced IFT88 knockdown (Figure 7B) had fewer and shorter (mean length, 0.6 ± 0.4 μm) primary cilia compared with control cells (mean length, 4.3 ± 0.7 μm) (Figure 7C). Doxycycline alone did not alter the length of primary cilia (Figure 7C). In contrast, cells that overexpressed IFT88 had (Figure 7E) significantly longer primary cilia (2.4 ± 0.5 μm) compared with cells transduced with empty vector (mean cilium length, 0.6 ± 0.2 μm) (Figure 7F,G). These results indicate that IFT88 availability is a limiting factor in ciliary elongation.

### 3.6 | Aldosterone-induced increase in collecting duct principal cell size depends on the integrity of the primary cilia

There is experimental evidence that aldosterone induces hypertrophy of CD principal cells,[13] while the primary cilia have been to participate in renal epithelial cell volume control.[18,19] To determine whether primary cilia are involved in the aldosterone-induced increase in cell size, we compared ciliated and non-ciliated cells under control conditions and after 24 hours of exposure to aldosterone (Figure 8). The percentage of ciliated $mCCD_{cl1}$ cells with a volume of >500 $\mu m^3$ increased from 43% to 72% in response to aldosterone treatment (Figure 8A). In contrast, the cell volume of $mCCD_{cl1}$ cells that were deciliated by doxycycline-induced IFT88 knockdown did not change in response to aldosterone treatment. Notably, IFT88 silencing caused the percentage of cells with a volume >1000 $\mu m^3$ to increase slightly from 5% in WT cells to 19% among IFT88KD cells (Figure 8A), which supports previous studies.[36] These results suggest that primary cilia are necessary for the aldosterone-induced increase in CD principal cell size (Figure 8B).

## 4 | DISCUSSION

Primary cilia of nondividing cells are dynamic structures, which continue to grow even after they are fully developed. Although ciliary length is defined by the cell type, it is regulated by environmental stimuli and may modulate the functional activity of the organelle.[4,37,38] In the kidney, the length of primary cilia is regulated by via an adaptive mechanism in response to changes in glomerular filtration rate (GFR) and, therefore, electrolyte delivery to the ASDN.[37,39,40] For instance, unilateral nephrectomy,

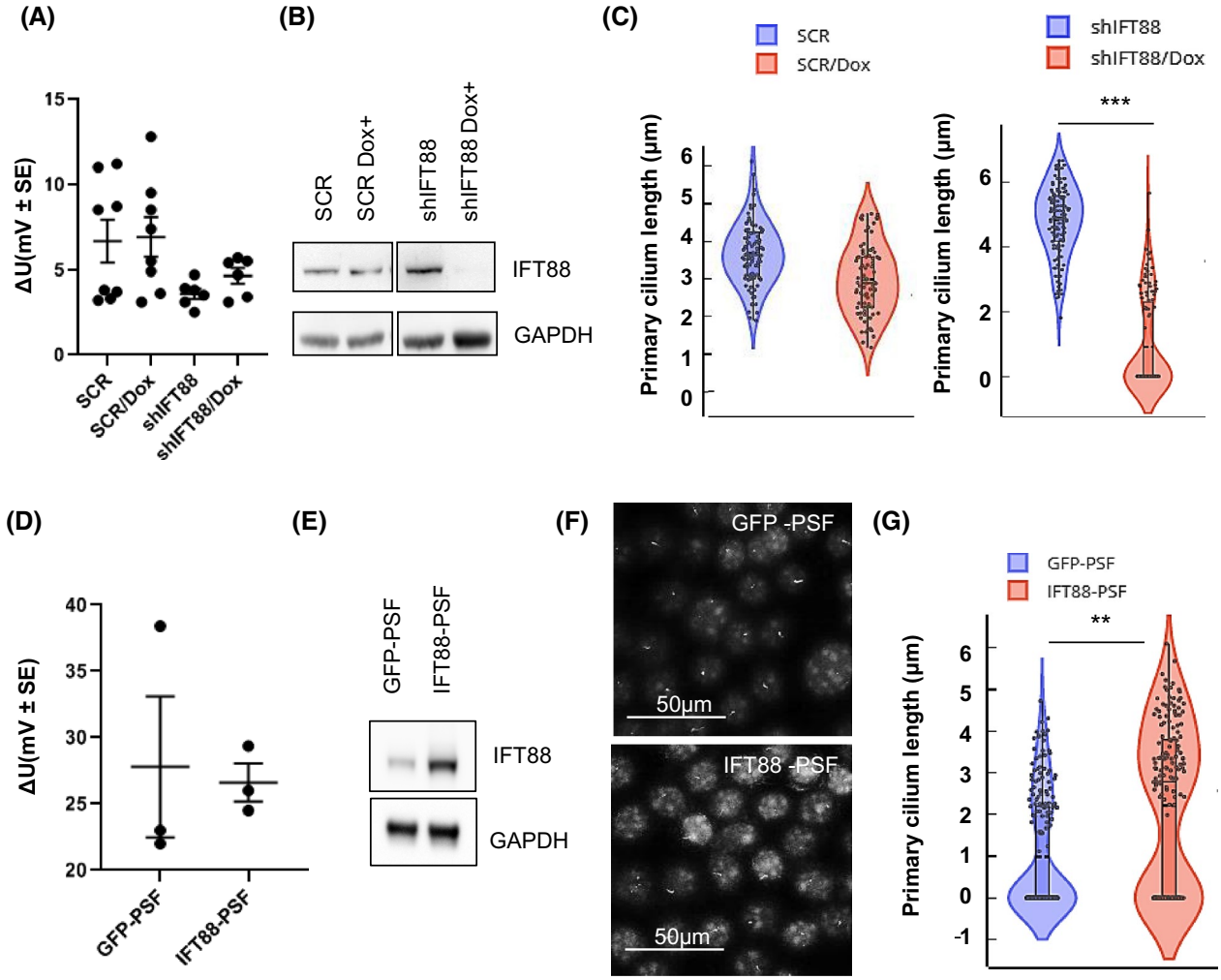


**FIGURE 7** Availability of IFT88 limits elongation of primary cilia in collecting duct principal cells. After transduction with lentiviruses encoding doxycycline-inducible scrambled shRNA (SCR) or shRNA targeting IFT88, $mCCD_{cl1}$ cells were grown to confluence in the presence (Dox) or absence (Ctl) of 0.5 μg/mL doxycycline for 5 days. A, Transepithelial potential difference measured in eight filters. Inducible silencing of IFT88 did not alter transepithelial potential difference. Each point represents a single measurement and bars represent mean ± standard error of the mean. B, Representative western blot from four independent experiments showing that shIFT88 caused almost complete knockdown of IFT88. C, Cells were fixed and stained with antibodies against acetylated α-tubulin to visualize primary cilia. Violin plot showing repartition of primary cilia by length with 250-300 cilia per condition. Results are from four independent experiments. Points represent the length of a single cilia and bars represent mean ± standard deviation. (D-G) $mCCD_{cl1}$ cells were transduced with lentiviruses encoding green fluorescent protein (GFP-PSF) or IFT88 (IFT88-PSF). D, Transepithelial potential difference measured in three filters. Each point represents a single measurement and bars represent mean ± standard error of the mean. E, Representative western blot of total cell lysate confirming IFT88 overexpression in IFT88-PSF cells compared with GFP-PSF cells. Cells were fixed and stained with antibodies against acetylated α-tubulin to visualize primary cilia. F, Representative summarized z-stacks from three independent experiments. G, Violin plot showing repartition of primary cilia by length with about 300 cilia per condition. Results are from three independent experiments. Points represent the length of a single cilia and bars represent mean ± standard deviation. Statistical analysis was performed by two-tailed Student's *t* test. $*P < .05$

which is associated with increased GFR and tubular $Na^+$ delivery, leads to ciliary elongation in epithelial cells of the remnant kidney.[42] Conversely, acute kidney injury which results in decreased GFR and, therefore, $Na^+$ delivery to renal tubule epithelial cells causes primary cilium shortening via reactive oxygen species/oxidative stress response mechanism.[37,39] The present study demonstrates that primary cilium length is linked to transepithelial $Na^+$ transport, independent of ENaC expression levels. This suggests that the GFR-related changes in primary cilium length relies, at least in part, on alteration of intracellular $Na^+$ influx and/or concentration. Primary cilia play a role in the macula densa-mediated regulation of $Na^+$ excretion,[43] and deletion of primary cilia leads to a 40% increase in tubuloglomerular feedback response and a subsequent reduction in GFR.[44]

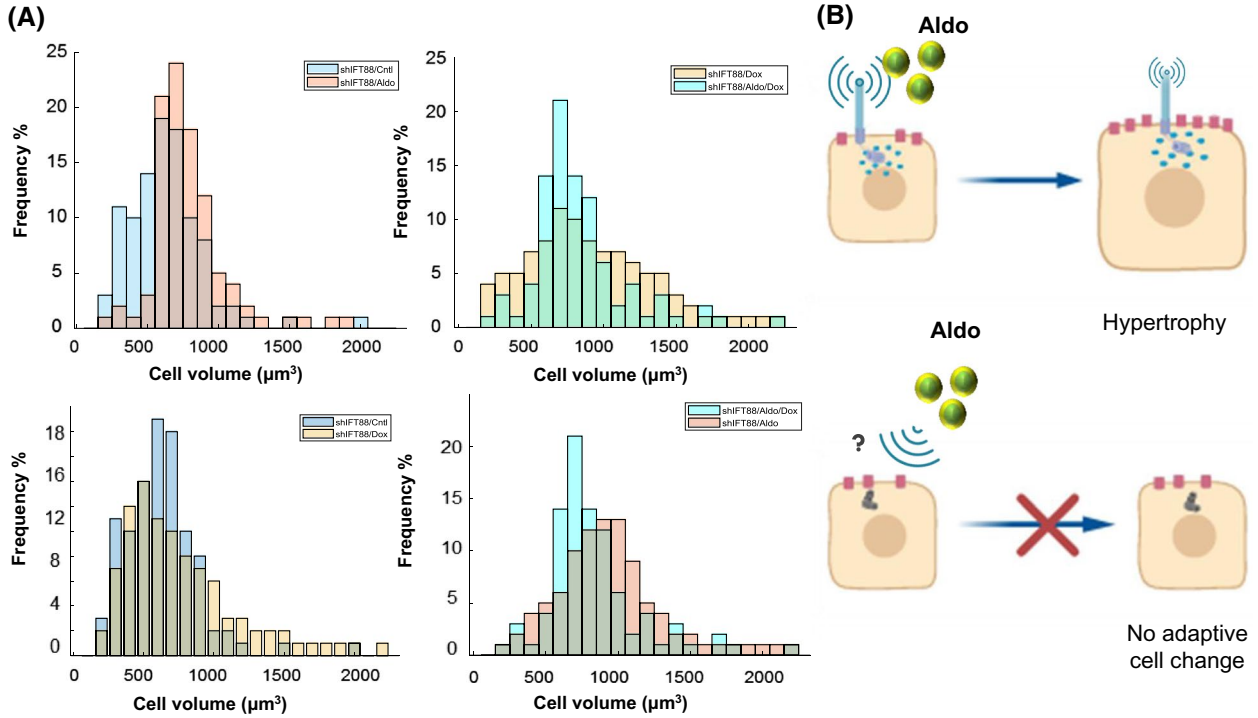


**FIGURE 8** Aldosterone induces cilium-regulated hypertrophy in collecting duct principal cells. A, Cell volume distribution of $mCCD_{cl1}$ cells transduced with lentiviruses encoding doxycycline-inducible scrambled shRNA (SCR) or shRNA targeting IFT88 (shIFT88) and grown to confluence in the presence (Dox) or absence (Ctl) of 0.5 μg/mL doxycycline for 5 days. Cells were then incubated in serum- and hormone-deprived medium for 24 hours in the absence (0 hours Aldo) or presence of $10^{-6}$ M aldosterone (Aldo) for 24 hours. The cell volume of individual cells was measured on three-dimensional reconstructions of z-stack images (see Video 1 and Section 2). A total of 400-600 cells from three independent experiments was measured for each condition. B, Schematic representation of the working model. Aldosterone-induced CD principal cell hypertrophy is prevented by disruption of primary cilia

In renal epithelial cells, the primary cilia are considered to have a mechanosensory function, which is important in the fluid shear stress response.[45,46] The entire ciliary compartment (cilioplasm) acts as a signal transduction platform linking many signaling pathways such as calcium and cAMP, mTOR, sonic hedgehog, PDGF, Wnt, Janus kinase/signal transducers, and activators of transcription, and mitogen-activated protein kinase-1 signaling pathways,[5,16,46,48] in which the cellular response to external stimuli correlates with the change in ciliary length.[47,48] The ciliary LKB1 module regulates macrophage recruitment and kidney chemokine signaling by downregulating CCL2 expression in tubular cells and is therefore implicated in ADPKD.[50] Activation of signaling pathways may be controlled by ciliary length because the number of signaling units contained within the organelle and/or mechanical properties of the primary cilia will be affected by the length. Indeed, longer cilia are more elastic and, therefore, susceptible to bending by tubular flow, which regulates cell mechanosensitivity.[51] This creates an additional level of signaling regulation via mechanotransduction pathways.[52,53] The changes in ciliary length that we observed may also regulate $Na^+$ reabsorption through paracrine purinergic signaling.[46,54,55] One can speculate that aldosterone-stimulated ciliary elongation is part of the negative feedback–mediated inhibition of ENaC in response to ATP release.[57]

In the present study, we demonstrate that changes in abundance of IFT88, a component of the ciliary building machinery responsible for anterograde transport along ciliary microtubules, are associated with variations in length of primary cilia. Complete or partial silencing of IFT88 resulted in the absence or shortening of primary cilia, respectively, while overexpression resulted in longer primary cilia. Therefore, aldosterone-induced ciliary elongation may be caused by increased IFT88 abundance due to inhibition of protein degradation. IFT88 has been shown to regulate prorenin and urinary angiotensin II levels, indicating activation of the intrarenal renin-angiotensin system (RAS),[58] which suggests that primary cilia may play a role in local RAS activation is response to aldosterone exposure.

The present study provides insight into the interplay between aldosterone and the primary cilia in the regulation of the size of CD principal cells. The effect of mTOR activity on cell size has been previously described as hypertrophic adaptive response.[18,59] Here, we describe the importance of the primary cilia in aldosterone-mediated cell size regulation, an adaptive phenomenon that has

been known for decades but remains enigmatic.[13] Larger cells have larger apical surfaces incorporating more ENaC channels and larger basolateral surfaces containing more Na-K-ATPase units; two features that were observed following sustained aldosterone stimulation. In addition, larger cells may contain more mitochondria owing to their increased energy demand. Control of cell size may rely on the modulation of autophagy as well as mTORC and AMPK pathways by the primary cilia.[36] Although our experiments were performed under static conditions, while in vivo CD principal cells are exposed to a luminal fluid flow, the physiological changes that we observed in $mCCD_{cl1}$ cells subjected to chronic orbital flow (which mimics luminal tubular flow) were independent of primary cilia integrity.

In conclusion, we demonstrate adaptive lengthening of primary cilia in response to stimulation of transepithelial $Na^+$ transport. Our results confirm that primary cilia are structurally dynamic cellular organelles. This morphological change is brought about, at least in part, by inhibition of IFT88 degradation. Our results highlight the correlation between integrity of the primary cilia and hypertrophic cell size increase in response to increased $Na^+$ transport. Thus, we propose that elongation of the primary cilia participates in this adaptive process.

## ACKNOWLEDGMENTS

The authors thank Dr. Sergei Startchik, Dr. Suresh Ramakrishnan, and Aarti Krishnan for their help with data analysis and advices on data presentation throughout the preparation of this article. This work was supported by the National Center of Competence in Research Kidney Control of Homeostasis a Swiss National Science Foundation grant 31003A_156736/1 and 31003A_175471/1 and a Fondation Ernst et Lucie Schmidheiny grant to EF.

## CONFLICT OF INTEREST

The authors have no conflicts of interest to declare.

## AUTHOR CONTRIBUTIONS

O. Komarynets designed research, performed experiments, analyzed data and wrote this paper, A. Chassot, E. Bernabeu, J. Czogalla, I. Roth, and N. Liaudet performed experiments and analyzed data, F. Prodon performed experiments, J. Loffing contributed new reagents, E. Feraille designed research and wrote this paper.

## REFERENCES

1. Satir P, Pedersen LB, Christensen ST. The primary cilium at a glance. *J Cell Sci*. 2010;123:499-503.
2. Davenport JR, Yoder BK. An incredible decade for the primary cilium: a look at a once-forgotten organelle. *Am J Physiol Renal Physiol*. 2005;289:F1159-F1169.
3. Bhogaraju S, Engel BD, Lorentzen E. Intraflagellar transport complex structure and cargo interactions. *Cilia*. 2013;2:10.
4. Avasthi P, Marshall WF. Stages of ciliogenesis and regulation of ciliary length. *Differentiation*. 2012;83:S30-S42.
5. Malicki JJ, Johnson CA. The cilium: cellular antenna and central processing unit. *Trends Cell Biol*. 2016;2:126-140.
6. Barker AR, Thomas R, Dawe HR. Meckel-Gruber syndrome and the role of primary cilia in kidney, skeleton, and central nervous system development. *Organogenesis*. 2014;10:96-107.
7. Nauli SM, Alenghat FJ, Luo Y, et al. Polycystins 1 and 2 mediate mechanosensation in the primary cilium of kidney cells. *Nat Genet*. 2003;33:129-137.
8. Fliegauf M, Benzing T, Omran H. When cilia go bad: cilia defects and ciliopathies. *Nat Rev Mol Cell Biol*. 2007;8:880-893.
9. Benmerah A, Durand B, Giles RH, et al. The more we know, the more we have to discover: an exciting future for understanding cilia and ciliopathies. *Cilia*. 2015;4:5.
10. Kohli P, Höhne M, Jüngst C, et al. The ciliary membrane-associated proteome reveals actin-binding proteins as key components of cilia. *EMBO Rep*. 2017;18:1521.
11. Boron WF, Boulpaep EL. *Medical physiology: a cellular and molecular approach*. Philadelphia, PA: Saunders/Elsevier; 2009.
12. Wall SM, Weinstein AM. Cortical distal nephron Cl(-) transport in volume homeostasis and blood pressure regulation. *Am J Physiol Renal Physiol*. 2013;305:F427-F438.
13. Wade JB, Stanton BA, Field MJ, Kashgarian M, Giebisch G. Morphological and physiological responses to aldosterone: time course and sodium dependence. *Am J Physiol*. 1990;259: F88-F94.
14. Praetorius HA, Spring KR. Removal of the MDCK cell primary cilium abolishes flow sensing. *J Membr Biol*. 2003;191:69-76.
15. Carrisoza-Gaytán R, Wang L, Schreck C, Kleyman TR, Wang W-H, Satlin LM. The mechanosensitive BKα/β1 channel localizes to cilia of principal cells in rabbit cortical collecting duct (CCD). *Am J Physiol Renal Physiol*. 2017;312:F143-F156.
16. Besschetnova TY, Kolpakova-Hart E, Guan Y, Zhou J, Olsen BR, Shah JV. Identification of signaling pathways regulating primary cilium length and flow-mediated adaptation. *Curr Biol*. 2010;20:182-187.
17. Olteanu D, Yoder BK, Liu W, et al. Heightened epithelial Na+ channel-mediated Na+ absorption in a murine polycystic kidney disease model epithelium lacking apical monocilia. *Am J Physiol Cell Physiol*. 2006;290:C952-C963.
18. Boehlke C, Kotsis F, Patel V, et al. Primary cilia regulate mTORC1 activity and cell size through Lkb1. *Nat Cell Biol*. 2010;12:1115-1122.
19. Orhon I, Dupont N, Zaidan M, et al. Primary-cilium-dependent autophagy controls epithelial cell volume in response to fluid flow. *Nat Cell Biol*. 2016;18:657-667.
20. Canonica J, Sergi C, Maillard M, et al. Adult nephron-specific MR-deficient mice develop a severe renal PHA-1 phenotype. *Pflugers Arch*. 2016;468:895-908.
21. Czogalla J, Vohra T, Penton D, Kirschmann M, Craigie E, Loffing J. The mineralocorticoid receptor (MR) regulates ENaC but not NCC in mice with random MR deletion. *Pflugers Arch*. 2016;468:849-858.
22. Gaeggeler HP, Gonzalez-Rodriguez E, Jaeger NF, et al. Mineralocorticoid versus glucocorticoid receptor occupancy mediating aldosterone-stimulated sodium transport in a novel renal cell line. *J Am Soc Nephrol*. 2005;16:878-891.
23. Wang Y-B, Leroy V, Maunsbach AB, et al. Sodium transport is modulated by p38 kinase-dependent cross-talk between ENaC and

Na, K-ATPase in collecting duct principal cells. *J Am Soc Nephrol*. 2014;25:250-259.
24. Ernandez T, Udwan K, Chassot A, Martin PY, Feraille E. Uninephrectomy and apical fluid shear stress decrease ENaC abundance in collecting duct principal cells. *Am J Physiol Renal Physiol*. 2017;314:F763-F772.
25. Sullivan LM, Weinberg J, Keaney JF Jr. Common statistical pitfalls in basic science research. *J Am Heart Assoc*. 2016;5:e004142.
26. Bens M, Vallet V, Cluzeaud F, et al. Corticosteroid-dependent sodium transport in a novel immortalized mouse collecting duct principal cell line. *J Am Soc Nephrol*. 1999;10:923-934.
27. Rafestin-Oblin ME, Fagart J, Souque A, Seguin C, Bens M, Vandewalle A. 11beta-hydroxyprogesterone acts as a mineralocorticoid agonist in stimulating Na+ absorption in mammalian principal cortical collecting duct cells. *Mol Pharmacol*. 2002;62:1306-1313.
28. Orhon I, Dupont N, Pampliega O, Cuervo AM, Codogno P. Autophagy and regulation of cilia function and assembly. *Cell Death Differ*. 2015;22:389-397.
29. Wang S, Livingston MJ, Su Y, Dong Z. Reciprocal regulation of cilia and autophagy via the MTOR and proteasome pathways. *Autophagy*. 2015;11:607-616.
30. Lang F, Pearce D. Regulation of the epithelial Na+ channel by the mTORC2/SGK1 pathway. *Nephrol Dial Transplant*. 2016;31:200-205.
31. Ivanova EA, van den Heuvel LP, Elmonem MA, et al. Altered mTOR signalling in nephropathic cystinosis. *J Inherit Metab Dis*. 2016;39:457-464.
32. Fantus D, Rogers NM, Grahammer F, Huber TB, Thomson AW. Roles of mTOR complexes in the kidney: implications for renal disease and transplantation. *Nat Rev Nephrol*. 2016;12:587-609.
33. Chen Z, Dong H, Jia C, et al. Activation of mTORC1 in collecting ducts causes hyperkalemia. *J Am Soc Nephrol*. 2014;25:534-545.
34. Sanchez I, Dynlacht BD. Cilium assembly and disassembly. *Nat Cell Biol*. 2016;18:711-717.
35. Malicki J, Avidor-Reiss T. From the cytoplasm into the cilium: bon voyage. *Organogenesis*. 2014;10:138-157.
36. Orhon I, Dupont N, Zaidan M, et al. Primary-cilium-dependent autophagy controls epithelial cell volume in response to fluid flow. *Nat Cell Biol*. 2016;18:657.
37. Kim JI, Kim J, Jang HS, Noh MR, Lipschutz JH, Park KM. Reduction of oxidative stress during recovery accelerates normalization of primary cilia length that is altered after ischemic injury in murine kidneys. *Am J Physiol Renal Physiol*. 2013;304:F1283-F1294.
38. O'Connor AK, Malarkey EB, Berbari NF, et al. An inducible CiliaGFP mouse model for in vivo visualization and analysis of cilia in live tissue. *Cilia*. 2013;2:8.
39. Han SJ, Jang HS, Seu SY, et al. Hepatic ischemia/reperfusion injury disrupts the homeostasis of kidney primary cilia via oxidative stress. *Biochem Biophys Acta*. 2017;1863:1817-1828.
40. Park KM. Can tissue cilia lengths and urine cilia proteins be markers of kidney diseases? *Chonnam Med J*. 2018;54:83-89.
41. Wang S, Dong Z. Primary cilia and kidney injury: current research status and future perspectives. *Am J Physiol Renal Physiol*. 2013;305:F1085-F1098.
42. Han SJ, Jang HS, Kim JI, Lipschutz JH, Park KM. Unilateral nephrectomy elongates primary cilia in the remaining kidney via reactive oxygen species. *Sci Rep*. 2016;6:22281.
43. Wang L, Shen C, Liu H, et al. Shear stress blunts tubuloglomerular feedback partially mediated by primary cilia and nitric oxide at the macula densa. *Am J Physiol Regul Integr Comp Physiol*. 2015;309:R757-R766.
44. Song J, Wang L, Fan F, et al. Role of the primary cilia on the macula densa and thick ascending limbs in regulation of sodium excretion and hemodynamics. *Hypertension*. 2017;70:324-333.
45. Rodat-Despoix L, Delmas P. Ciliar functions in the nephron. *Pflugers Arch*. 2009;458:179-187.
46. Praetorius HA, Leipziger J. Primary cilium-dependent sensing of urinary flow and paracrine purinergic signaling. *Semin Cell Dev Biol*. 2013;24:3-10.
47. Atkinson KF, Kathem SH, Jin X, et al. Dopaminergic signaling within the primary cilia in the renovascular system. *Front Physiol*. 2015;6:103.
48. Pala R, Alomari N, Nauli S. Primary cilium-dependent signaling mechanisms. *International Journal of Molecular Sciences*. 2017;18(11):2272.
49. Jin X, Mohieldin AM, Muntean BS, et al. Cilioplasm is a cellular compartment for calcium signaling in response to mechanical and chemical stimuli. *Cell Mol Life Sci*. 2014;71:2165-2178.
50. Viau A, Bienaimé F, Lukas K, et al. Cilia-localized LKB1 regulates chemokine signaling, macrophage recruitment, and tissue homeostasis in the kidney. *EMBO J*. 2018;37:e98615.
51. Spasic M, Jacobs CR. Lengthening primary cilia enhances cellular mechanosensitivity. *Eur Cell Mater*. 2017;33:158-168.
52. Nag S, Resnick A. Biophysics and biofluid dynamics of primary cilia: evidence for and against the flow-sensing function. *Am J Physiol Renal Physiol*. 2017;313:F706-F720.
53. Raghavan V, Weisz OA. Discerning the role of mechanosensors in regulating proximal tubule function. *Am J Physiol Renal Physiol*. 2016;310:F1-F5.
54. Vallon V, Rieg T. Regulation of renal NaCl and water transport by the ATP/UTP/P2Y2 receptor system. *Am J Physiol Renal Physiol*. 2011;301:F463-F475.
55. Wildman SS, Marks J, Turner CM, et al. Sodium-dependent regulation of renal amiloride-sensitive currents by apical P2 receptors. *J Am Soc Nephrol*. 2008;19:731-742.
56. Pluznick JL, Caplan MJ. Chemical and physical sensors in the regulation of renal function. *Clin J Am Soc Nephrol*. 2015;10:1626-1635.
57. Gorelik J, Zhang Y, Sánchez D, et al. Aldosterone acts via an ATP autocrine/paracrine system: the Edelman ATP hypothesis revisited. *Proc Natl Acad Sci USA*. 2005;102:15000-15005.
58. Saigusa T, Dang Y, Bunni MA, et al. Activation of the intrarenal renin-angiotensin-system in murine polycystic kidney disease. *Physiol Rep*. 2015;3:e12405.
59. Mounier R, Lantier L, Leclerc J, Sotiropoulos A, Foretz M, Viollet B. Antagonistic control of muscle cell size by ampk and mtorc1. *Cell Cycle*. 2011;10:2640-2646.

## SUPPORTING INFORMATION

Additional supporting information may be found online in the Supporting Information section.

**How to cite this article:** Komarynets O, Chassot A, Bernabeu E, et al. Aldosterone controls primary cilium length and cell size in renal collecting duct principal cells. *The FASEB Journal*. 2020;34:2625–2640. https://doi.org/10.1096/fj.201901947R